



Effect of cooling rate on microstructure and tensile properties of powder metallurgy Ni-based superalloy

Han-hui DING^{1,2}, Guo-ai HE^{1,2}, Xin WANG^{1,2}, Feng LIU^{1,2}, Lan HUANG^{1,2}, Liang JIANG^{1,2}

1. State Key Laboratory of Powder Metallurgy, Central South University, Changsha 410083, China;

2. Powder Metallurgy Research Institute, Central South University, Changsha 410083, China

Received 1 November 2016; accepted 28 March 2017

Abstract: The effects of size distribution, morphology and volume fraction of γ' phase and grain size on tensile properties of powder processed Ni-based superalloy were investigated by using two different quenching methods. Oil quenching and air cooling were adopted with cooling rate of 183 °C/s and 4–15 °C/s, respectively. The experimental results show that the average size of the secondary γ' after oil quenching is 24.5 nm compared with 49.8 nm under air cooling, and corresponding volume fractions of γ' are 29% and 34%, respectively. Meanwhile, the average grain size remains nearly equivalent from both oil-quenching and air-cooling specimens. The tensile strength at room temperature is higher for the oil-quenched specimen than the equivalent from the air-cooled specimen, but the difference approaches each other as the temperature increases to 650 °C. The fractography clearly demonstrates that transgranular fracture governs the failure process at ambient temperature, in contrast to the intergranular fracture at 650 °C or even higher temperature. These two mechanical responses indicate the strengthening effects of γ' precipitates and grain boundary for polycrystalline Ni-based superalloys at different temperatures.

Key words: powder metallurgy Ni-based superalloy; cooling rate; tensile properties; γ' phase precipitate; fracture mechanism

1 Introduction

Polycrystalline Ni-based superalloys have been widely used for gas turbine disk of aircraft due to their excellent high temperature strength, fatigue and creep resistance, oxidation and corrosion resistance, superior microstructure stability and service reliability [1,2]. These striking mechanical performances upon elevated temperature have been primarily attributed to the ordered and coherent γ' precipitates with a disordered γ matrix. The microstructure of disk superalloys, especially in terms of the morphology, as well as the spatial and size distribution of γ' precipitates, plays a very important role in determining the mechanical properties [3,4].

The heat treatment of the turbine disk components is a crucial process for achieving an optimum microstructure and mechanical properties [5–7], which can be achieved by the typical processing of turbine disk blanks, termed as solution and aging treatment. The grain size and γ' precipitates are significantly affected by heat

treatment. Specimens heated to a supersolvus solution temperature usually can obtain coarse grain size bringing better crack growth resistance, but lower tensile strength [8]. So, it is necessary to improve the tensile property through the process of cooling or ageing treatment. Previous researches [9–11] show that the size distribution, morphology and volume fraction of γ' can be modified by cooling pathways in a controllable manner. Wherein, controlling of γ' precipitation through quenching greatly affects the final tensile properties, because the nucleation and growth kinetics of the precipitates strongly depend on the cooling rate during quenching. Many researchers [12–14] have studied the effect of different steady cooling rates on the γ' precipitates characteristics, showing that the higher cooling rate can obtain higher strength despite the tendency to crack.

In practice, the typical quenching media, i.e., water, oil, air, are utilized to cool down the alloys and produce the desirable mechanical properties. However, the cooling rate from near solvus temperature to low

temperature is nonlinear and hard to be quantitatively described, leading to the difficulty to establish the relationship between cooling rate and mechanical strength. In this work, we quantitatively investigated the cooling process by means of two kinds of cooling media, and systematically characterized the tensile properties corresponding to two different cooling rates in order to explain the mechanism underpinning the tensile failure process.

2 Experimental

2.1 Materials

A powder metallurgy (P/M) processed Ni-based superalloy, designated as CSU-A1, was used in this work. Table 1 lists its nominal composition. The master alloy was melted by vacuum inducing melting followed by gas atomization and hot isostatic pressing (HIP) compaction. Later, the billet bar was hot-extruded (HEX) with a reduction ratio of 12:1. The tensile specimens were cut from the extruded bar and the geometry of specimen is depicted in Fig. 1.

Table 1 Nominal composition of CSU-A1 alloy (mass fraction, %)

Co	Cr	Mo	W	Al	Ti
26	13	4	4	3.3	4.0
Nb	Hf	C	B	Zr	Ni
0.9	0.2	0.04	0.03	0.04	Bal.

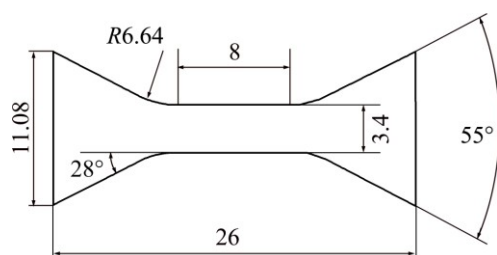


Fig. 1 Geometry of tensile sample (unit: mm)

2.2 Solution temperature tests

Prior to the heat treatment, it was critical to determine the solvus temperature of γ' phase for a new P/M superalloy. Different thermal analysis (DTA), thermodynamic calculation and metallographic analysis method were utilized to determine the phase precipitation temperature separately. The DTA test was conducted using an ultra-high temperature thermo gravimetric analysis (Setsys Evo). The sample sizes used were 2.5 mm \times 2.5 mm \times 2.5 mm and the heating/cooling rate during the test was 10 °C/min. The thermodynamic calculation was performed using the Thermo-Calc software with the TTNi8 database. Metallographic analysis method was conducted by heating up the

samples to a series of temperature including 1110, 1130, 1140, 1150 and 1170 °C and exposing for 1 h in a electric-resistance tube furnace, and finally followed by water quenching to remain the original solution structure.

2.3 Heat treatment and cooling rate tests

Tensile samples were cut to sizes of about 26 mm \times 11 mm \times 2 mm shown in Fig. 1 by a wire electrolytic-discharge machine and divided into two groups by different cooling approaches. The specimens were enclosed in a silica tube and back-filled with nitrogen to avoid oxidation and elemental evaporation. Heat treatment consists of a supersolvus treatment of 1165 °C for 1 h and a subsequent quenching in the oil or air, respectively. Both two groups of specimens were aged for 8 h at temperature of 815 °C finally. Monitor thermocouples were welded on the specimen surface before heating up. The measurement of cooling rate was performed using a temperature monitor (RDXL8, OMEGA) with a record frequency of 2 Hz.

2.4 Tensile property tests

The tensile tests were performed at the temperatures of 25, 400, 650, 700 and 750 °C. Prior to tensile test, the samples were heated to target temperature inside the furnace and then soaked for 15 min. The loading strain rate is set up to 10^{-4} s $^{-1}$ which was controlled by crosshead using the electronic universal testing machine (UTM5105, SUNS). Each test was repeated at least twice to guarantee the reliability of the experimental measurement. The tensile failure for all the specimens occurs within the gage length.

2.5 Microstructure characterization

Prior to the microstructure observation, the specimens were manually ground up to 1000-grits sand paper and polished with 0.05 μ m alumina suspension. Subsequently, vibratory polishing was used to achieve high-quality surface. In order to observe the grain boundary and precipitates, the specimens were etched using different etchants, as shown in Table 2. Microstructure analyses of the samples were performed by optical microscopy (OM, DM4000M, Leica) and scanning electron microscopy (SEM, QUANTA 650 FEG, FEI). The grain size was measured using electron back-scattered diffraction (EBSD, QUANTA 650 FEG, FEI) technique. Image post-processing software was

Table 2 Information for etching methods [15]

Enchant	Etching time/s	Microstructure
50 mL lactate + 30 mL nitrate + 2 mL HF	10~15	γ'
100 mL HCl + 100 mL alcohol + 5 g CuCl	60~90	Grain boundary

used to estimate the volume fraction and size distribution of γ' phase.

3 Results and discussion

3.1 Phase-transformation analysis and γ' solvus temperature determination

The γ' solvus and solidus temperatures determined by Thermo-Calc software were 1153 and 1262 °C. Table 3 shows the selected equilibrium thermodynamic data from calculation. The heat treatment window is 109 °C. The maximum γ' molar fraction would be 46% after aging at 815 °C which is normally supposed to be the volume fraction.

Table 3 Selected equilibrium thermodynamic data of CSU-A1 alloy

Liquidus temperature/ °C	Solidus temperature / °C	γ' solvus/ °C	γ' molar fraction at 815 °C/%	Heat treatment window/°C
1344	1262	1153	46	109

The DTA curve shows two distinct transition points and the corresponding tangent lines are depicted as shown in Fig. 2. The γ' solvus and solidus temperatures are measured to be 1140 and 1258 °C. Generally, DTA is a widely used technique to measure phase transformation, but typically accompanied with an error range of ± 25 °C compared with calculation value [16]. So, it is not precise enough to use the data from thermodynamic calculation and DTA for this alloy.

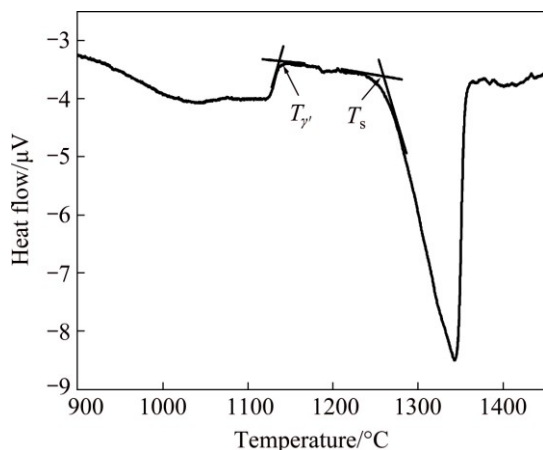


Fig. 2 DTA curve of CSU-A1 alloy

Moreover, the metallographic method is employed to verify the γ' solvus temperature, where different temperatures ranging from 1110 to 1170 °C are imposed to determine the solution temperature of γ' phase. Figure 3 shows the metallographic observation of γ' phase after solution treatment at different temperatures. In Figs. 3(a–c), the primary γ' phases lie on the grain

boundaries and its volume fraction decreases with increasing the solution temperature. As shown in Fig. 3(c), only a small amount of primary γ' phase can be detected, which means that γ' phase becomes dissolved at 1140 °C and can be related to the solvus temperature. With increasing the temperature further, the grain boundaries become more and more clean, which indicates that γ' phase dissolves completely, in accompany with the substantial grain growth. Therefore, the complete solution temperature of γ' phase is defined to be ranging from 1140 to 1150 °C.

3.2 Cooling rate and microstructure

3.2.1 Cooling rate

Oil quenching and air cooling have been widely used for cooling the samples. The difference of cooling rate between oil quenching and air cooling comes from their different thermal transfer coefficients. The derivative of cooling curve represents the cooling rate. Figure 4 shows the cooling curves corresponding to the oil quenching and air cooling, wherein the average cooling rates are measured to be 183 °C/s and 4–15 °C/s, respectively. Regarding the cooling behavior in air, cooling rate increases from 4 °C/s to maximum 15 °C/s at 950 °C, then later decreases as temperature drops. Generally, the temperature on the surface of samples is a dynamically balanced effect between heat absorption and release. Specifically, heat exchange occurred between the environment and sample surface, also from the inside to the surface of sample.

3.2.2 Effects of cooling rate on cooling precipitation

Upon supersolvus solution treatment, the primary γ' precipitates near the grain boundaries are completely dissolved. With the temperature decreasing, phase transformation in a form of γ' precipitation occurs within the grain interior. The morphology, the size and the volume fraction of γ' phase are closely related to the cooling rate. After aging treatment, small amount of tiny γ' phase will precipitate in the matrix, which is manifested as tertiary γ' precipitates. The existence of secondary and tertiary γ' phase is reported to substantially strengthen the high temperature performance.

The morphology of γ' phase before heat treatment is shown in Fig. 5(a). Fine precipitates are distributed inside the grains and a few large γ' phases can be found at the grain boundaries. By employing two different quenching methods, bimodal distribution in final γ' size and shape is achieved. The statistical result in Fig. 5(b) reveals that the size of γ' phase is generally located in the range of 20 and 150 nm, where the size of 60 nm occupies the dominated fraction. In addition, the bulk sizes of γ' phase at the grain boundary are measured as 300 nm \times 500 nm. After heat treatment, the γ' phase

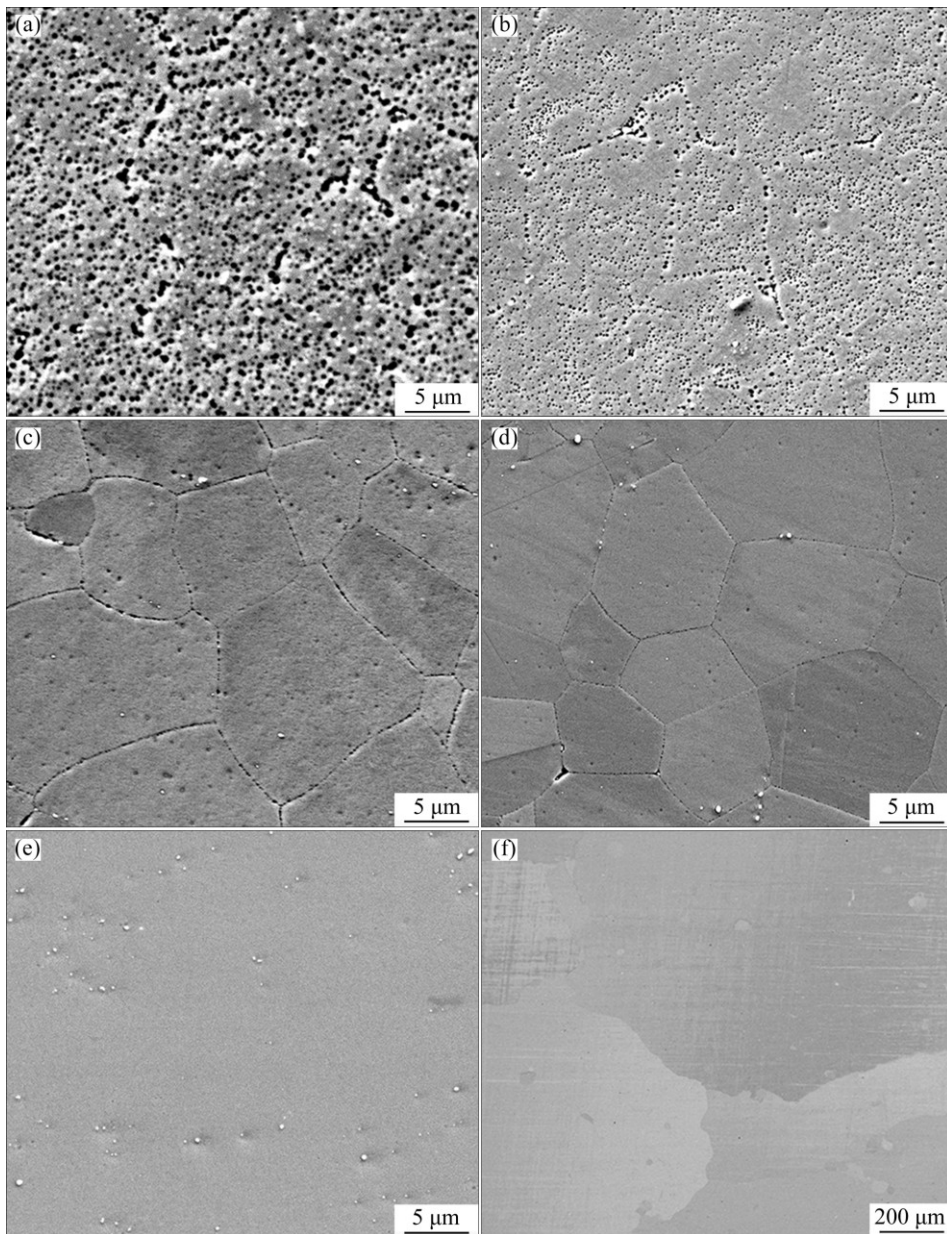


Fig. 3 Metallographic characterization of γ' phase after solution treatment at different solvus temperatures: (a) 1110 °C; (b) 1130 °C; (c) 1140 °C; (d) 1150 °C; (e, f) 1170 °C

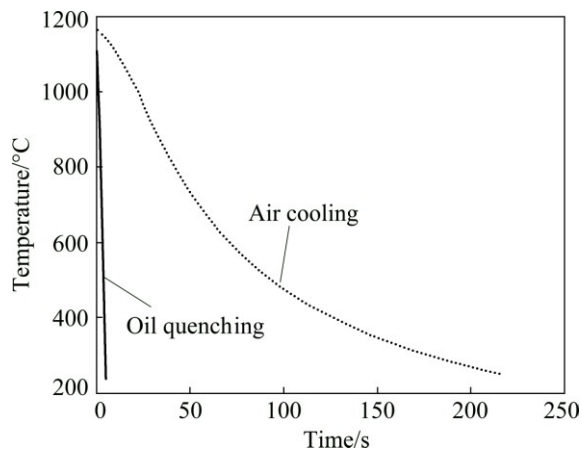


Fig. 4 Cooling curves with two quenching methods

would re-precipitate in the matrix, as shown in Figs. 5(c) and (e). Spherical and fine γ' phase is uniformly distributed in the matrix. For the case of air cooling, the diameter of γ' phase mainly ranges from 10 to 110 nm, as shown in Fig. 5(d). It behaves a bimodal distribution feature that consists of 15 and 45 nm. Larger γ' precipitate is supposed to form during the quenching process and grow up in the process of aging treatment, in companying with nucleation and growth of smaller γ' phase. The diameter of γ' phase through oil quenching is also shown in Fig. 5(f), which mainly ranges from 10 to 60 nm. The statistical chart shows a unimodal distribution and the most frequently occurred value is 20 nm. The volume fractions of γ' precipitates are 27%,

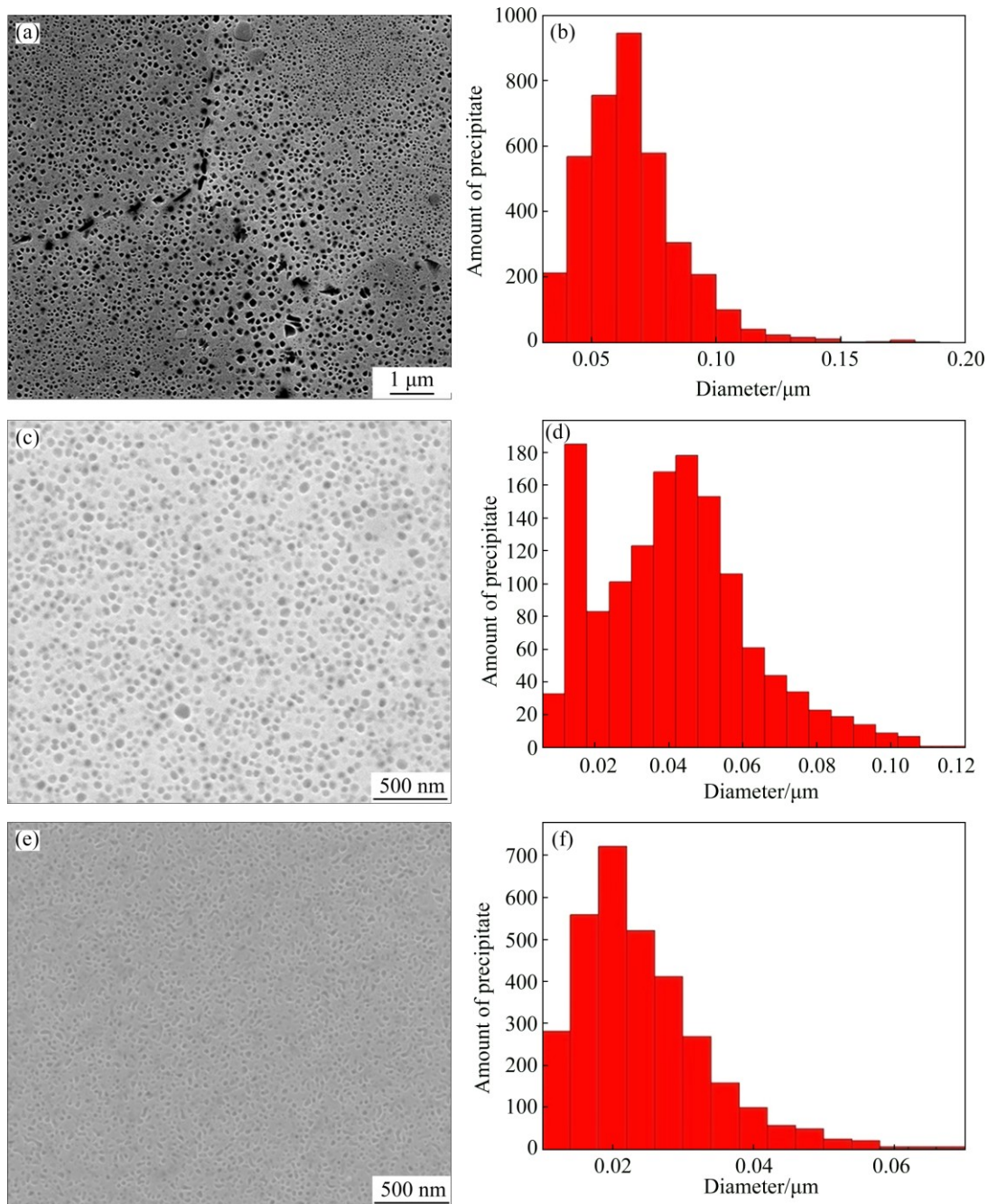


Fig. 5 Morphology and size distribution of γ' phase: (a, b) As-hexed; (c, d) Air cooling; (e, f) Oil quenching

34% and 29%, respectively. The γ' fraction in air-cooling state is higher than that in oil-quenching state mostly due to the longer time for γ' precipitates to grow up. All the measurements are summarized in Table 4.

The formation of γ' precipitates can be divided as three distinctly different stages while cooling from supersolvus temperature, i.e., nucleation, growth and coarsening. The nucleation of γ' precipitates depends on two competing mechanisms between Gibbs free energy generated by supersaturation in the matrix and the interface energy of new phase. In cooling process, the higher cooling rate will result in higher supersaturation and facilitates the formation of small γ' nucleus.

Moreover, faster cooling can suppress the formation of diffusion-controlled γ' , which strongly depends on the time and temperature, even though the interparticle spacing is smaller and short-distance diffusion is required. As a result, fast cooling generally relates to a larger amount of smaller cooling precipitates with a smaller interparticle spacing.

When the cooling rate slows down, the undercooling is smaller and accordingly the matrix supersaturation decreases. The size of first-burst γ' precipitates is bigger and the interparticle spacing is correspondingly larger. The precipitates grow with the short-distance diffusion but the long-distance diffusion is

unlikely to occur. So, there is a chance for the secondary supersaturation to be developed herein in the space of particles. Once the secondary supersaturation overcomes the nucleation barrier, the secondary burst of precipitate occurs with the synergetic effects of energy, structure and element.

3.2.3 Effects of cooling rate on grain size

Figure 6 shows the metallographic structures and Euler maps at different states. Equiaxed grains driven by recrystallization are achieved after hot extrusion, as shown in Figs. 6(a) and (b). The average grain size is measured as 12.5 μm. After heat treatment, ignorable grain growth is detected. The average grain size of specimens obtained from air cooling and oil quenching is

Table 4 Physical parameters of γ' phase

State	Cooling rate/ (°C·s ⁻¹)	Volume fraction/ %	Distribution interval of diameter/nm	Distribution peak(s) of diameter/nm	Average diameter/nm
As-hexed	–	27	35–150	60	67.0
Air cooling	4–15	34	10–110	15, 45	49.8
Oil quenching	183	29	10–60	20	24.5

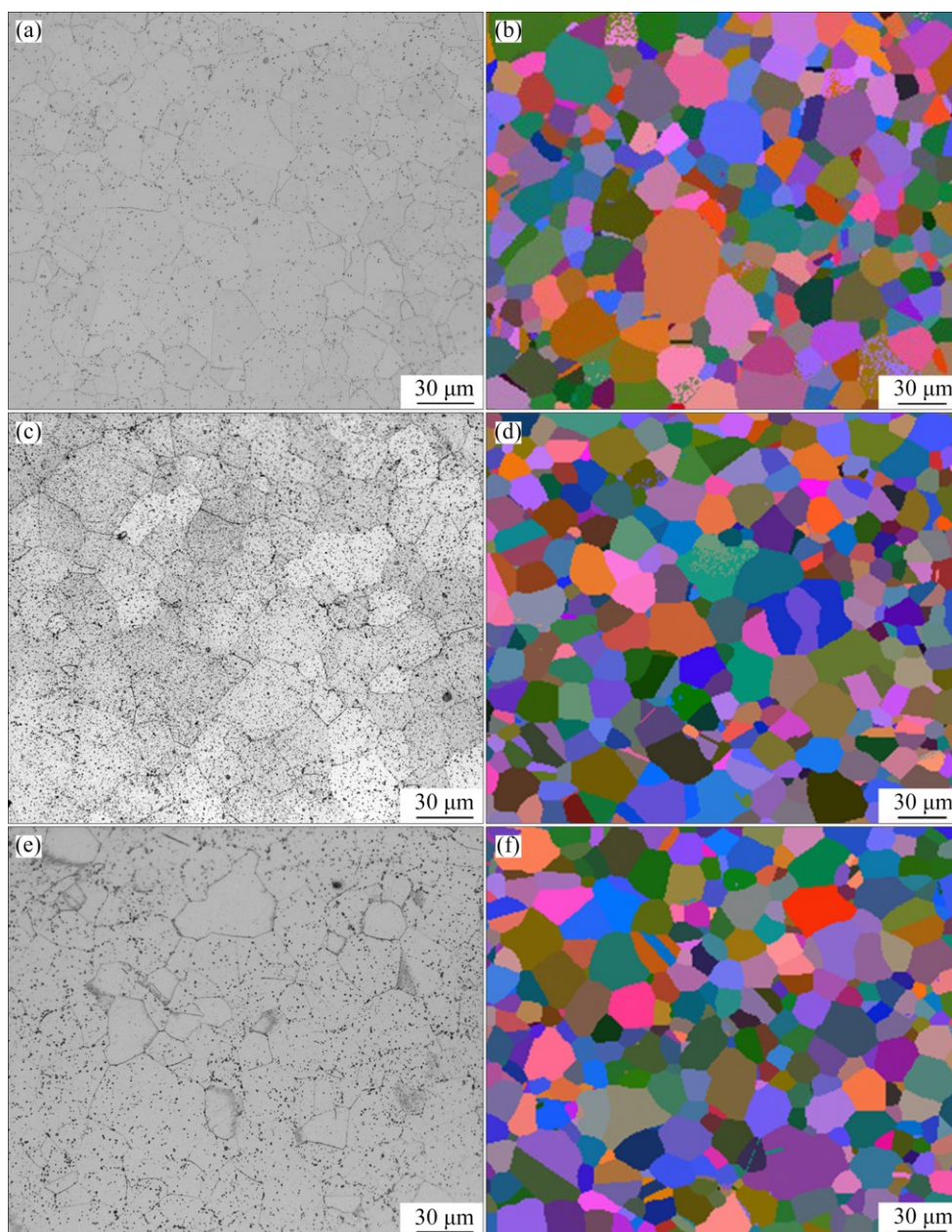


Fig. 6 Metallographic structure and Euler diagrams: (a, b) As-hexed; (c, d) Air cooling; (e, f) Oil quenching

determined to be 15 μm (c, d) and 13.5 μm (e, f) respectively, as shown in Fig. 7. The average grain size (equivalent circle diameter) through fast cooling turns out to be smaller than that of slow cooling. Most studies [17–19] show that the cooling rate will only determine the morphology and size distribution of γ' phase. There are few reports about the effects of cooling rate on the grain growth.

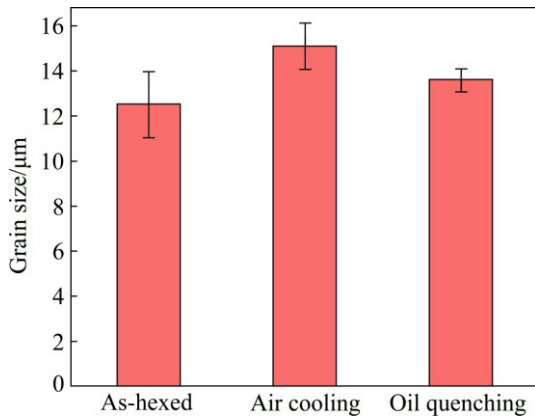


Fig. 7 Average grain size under different conditions

3.3 Tensile properties and fracture behavior

3.3.1 Tensile properties

Figure 8 reveals the dependence of yielding strength, ultimate tensile strength and ductility on the cooling rate upon different temperatures. For comparison, previous successfully-developed alloys, such as RENE 104, FGH96 alloys [13,20] are adopted from the documented literatures. For both two groups of alloys, the mechanical strength decreases with increasing the working temperature.

The yield strength, ultimate tensile strength and ductility of different alloys are shown in Fig. 8. The green line represents the third generation of Ni-based P/M superalloy, RENE 104. The blue one represents the second generation of Ni-based P/M superalloy, FGH96, after salt quenching. The ultimate strength of CSU_A1-OQ is higher than that of FGH96 but lower than that of RENE 104 at the medium and room temperatures, which is shown in Fig. 8(a).

Based on the results of mechanical test at 650 $^{\circ}\text{C}$, the tensile strength of oil-quenched specimen exceeds that of air-cooled process, yet, the difference of tensile strength between oil-quenched and air-cooled specimens becomes smaller with increasing the temperature. When the temperature is increased to 650 $^{\circ}\text{C}$, the ultimate tensile strength decreases sharply to 1200 MPa. At even higher temperature, the ultimate strength approaches each other for the oil-quenched and air-cooled specimens (Fig. 8(a)).

At room and medium temperatures, the yield strength of oil-quenched specimen is higher than that of

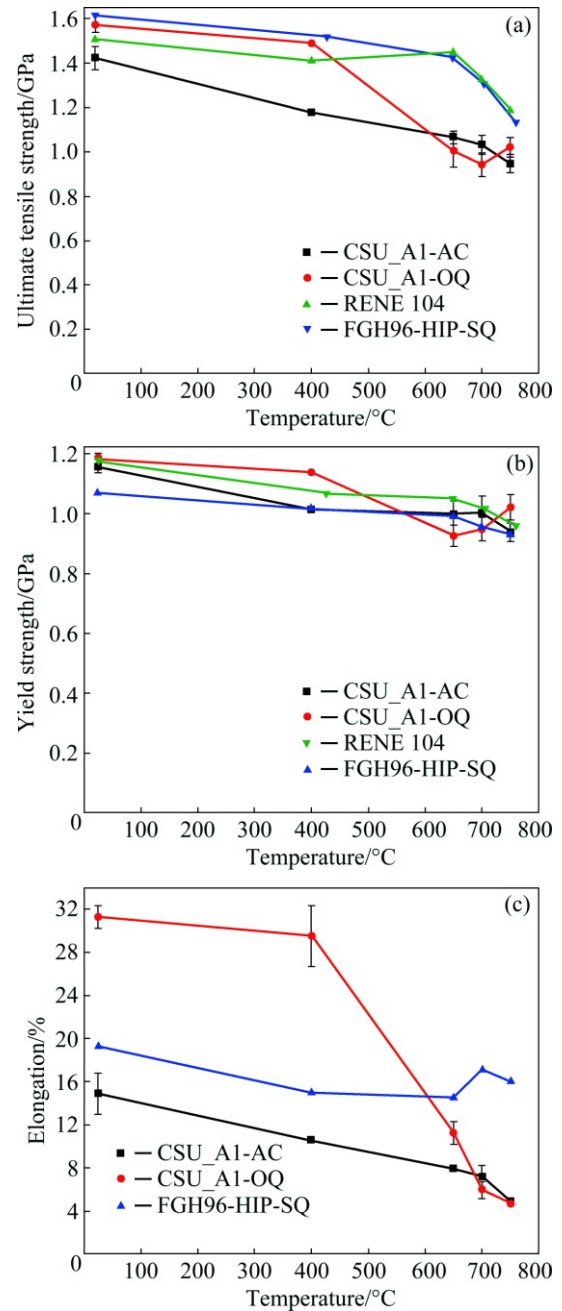


Fig. 8 Tensile properties of different alloys: (a) Ultimate tensile strength; (b) Yield strength; (c) Elongation

air-cooled one, as demonstrated in Fig. 8(b). When the temperature becomes higher, i.e., 650 $^{\circ}\text{C}$, the yield strength of oil-quenched alloy reduces 900 MPa which is very close to that of air-cooled counterpart. At room and medium temperatures, the fracture elongation of oil-quenched specimen is higher than that of air-cooled one. The result further shows that the higher temperature can substantially degrade the ductility, leading to the fact that the fracture elongation is approximately equivalent for both oil-quenched and air-cooled alloys.

According to the precipitation-hardening theory [21], when precipitate is small, it can be cut or

deformed by dislocations or weakly coupled dislocation pairs. There are six aspects of the particles that affect the cutting energy: coherency strain, stacking-fault energy, ordered structure, modulus effect, interfacial energy and morphology, and lattice-friction stress. Normally, the summation of these mechanisms leads to an increase in strength with particle size. However, when the particle size increases further, the cutting routine becomes very difficult, and the dislocations have to bypass the particles. After that, the strength actually decreases with the increase of the particle size. Hence, there is a critical particle size that offers the maximum resistance to dislocation motion. On the other hand, grain size plays an important role in strength according to the Hall–Petch relationship [22]. The strength decreases with grain size increasing at certain low temperatures.

Based on above results, the micromechanism can be explained as follows: at room and medium temperatures, the finer secondary γ' phases of oil-quenched alloy act as the leading role to carry on the plastic deformation due to the faster cooling rate. In contrast, the mechanical behavior is controlled and mediated by the grain boundary-related process. Therefore, various γ' phases derived from different cooling rates can impose weak effect on the deformation process, resulting in the approaching of mechanical strength and ductility.

3.3.2 Fracture behavior

Figure 9 presents the fractographic observation of the post-tensile alloy at room temperature, indicating that the macroscopic fracture is governed by planar-dominated crack. The inclined angle of fracture surface along with tensile axis equals 45° (Fig. 9(a)) and the crack initiates from the specimen surface. The microscale dimples (Fig. 9(b)) are the primary failure features and clearly demonstrate the role of γ' precipitates. At 400°C , the fracture plane is observed in Figs. 10(a) and (b) and fracture angle is 45° relative to the tensile direction. The micrometer-sized dimples and tearing ridges are ubiquitous, which shows that the plastic fracture dominates the deformation process.

At the higher temperature, from 650 to 750°C , the macroscopic fracture plane exhibits non-planar feature (Fig. 11(a)). The crack propagation pathway is intergranular fracture from the surface of specimen (Fig. 11(b)), and a large number of white nanoparticles can be detected. Figure 11(c) shows the crack propagation area and found that it mainly consists of fracture facets in a zigzag manner. This intergranular fracture demonstrates limited dimples on the surface. Similar to the behavior at the room temperature, the shear lip is formed by means of accumulation of shallow dimples (Fig. 11(d)).

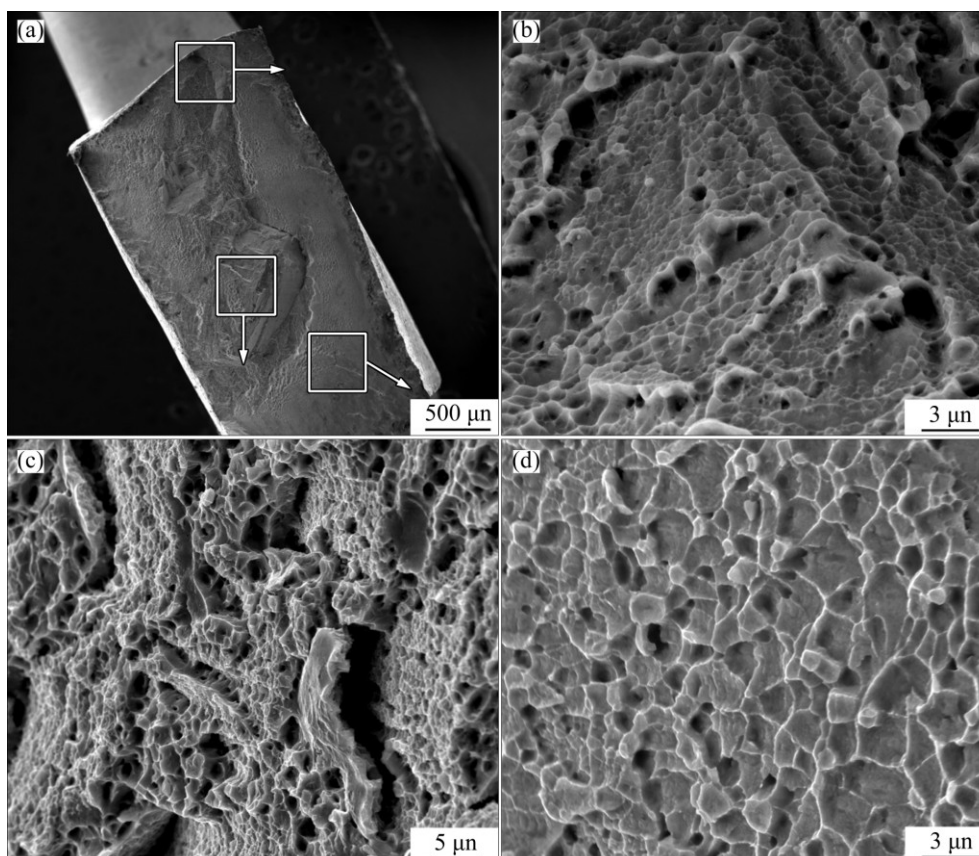


Fig. 9 Fractographs of tensile-fractured specimen at room temperature (as arrowed): (a) Macroscopic fracture; (b) Crack initiation; (c) Propagation area; (d) Shear lip

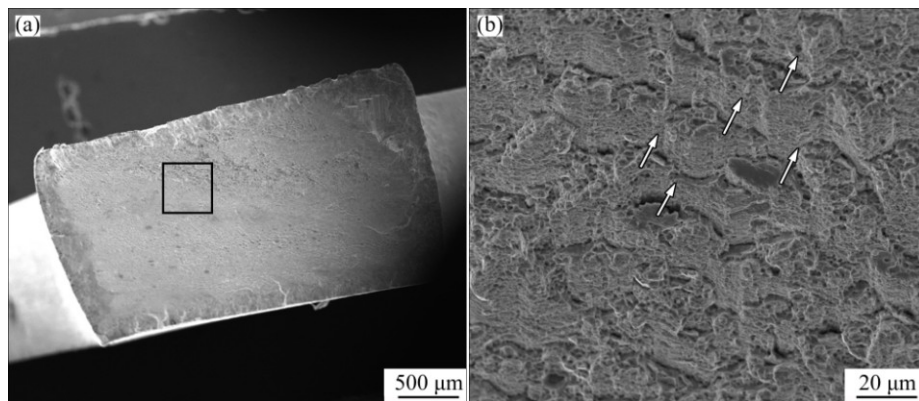


Fig. 10 Fractographs of tensile-fractured specimen at 400 °C: (a) Macroscopic fracture; (b) Micro fracture

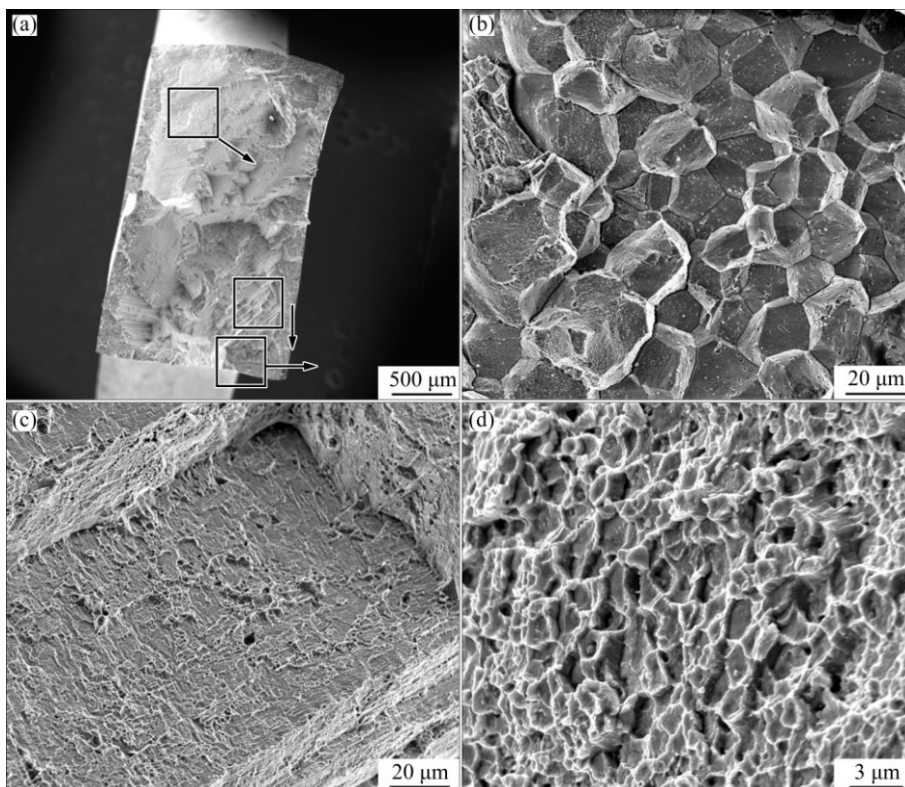


Fig. 11 Fractographs of tensile-fractured specimen at 650 °C (as arrowed): (a) Macroscopic fracture; (b) Crack initiation; (c) Propagation area; (d) Shear lip

4 Conclusions

1) Metallography observation provides an effective way to determine the phase transition temperature. The γ' solvus temperature for a new superalloy is experimentally determined to be 1140–1150 °C.

2) The cooling rates during oil quenching and air cooling are measured to be 183 and 4–15 °C/s, respectively. Uniform and fine γ' phase with an average size of 24.5 nm is obtained when the specimens are cooled by oil quenching, while bimodal distribution in γ' size ranging from 15 and 60 nm is detected in the specimens through air cooling.

3) For both oil-quenching and air-cooling specimens, the transgranular fracture governs the failure process at the ambient temperature. However, when the temperature is increased to 650 °C or higher, the crack propagation pathway becomes intergranular mode initiated from the specimen surface.

4) The ultimate tensile strength of oil quenching is obviously higher than that of air cooling at intermediate temperature. When the temperature becomes higher, the tensile strength of oil-quenched specimen degrades and approaches the equivalent of air cooling. The results show that the fracture begins with intergranular cracks at high temperature for both oil quenched and air cooled specimens.

References

- [1] POLLOCK T M, TIN S. Nickel-based superalloys for advanced turbine engines: Chemistry, microstructure and properties [J]. Journal of Propulsion & Power, 2006, 22(2): 361–374.
- [2] REED R C. The superalloys: Fundamentals and applications [M]. London: Cambridge University Press, 2006.
- [3] JIA C L, GE C C, YAN Q Z. Microstructure evolution and mechanical properties of disk superalloy under multiplex heat treatment [J]. Materials Science and Engineering A, 2016, 659: 287–294.
- [4] CHEN Y Q, FRANCIS E, ROBSONN J, PREUSS M, HAIGH S J. Compositional variations for small-scale gamma prime (γ') precipitates formed at different cooling rates in an advanced Ni-based superalloy [J]. Acta Materialia, 2015, 85: 199–206.
- [5] QIU C, WU X, MEI J, ANDRES P, VOICE W. Influence of heat treatment on microstructure and tensile behavior of a hot isostatically pressed nickel-based superalloy [J]. Journal of Alloys and Compounds, 2013, 578: 454–464.
- [6] LIU Chen-ze, LIU Feng, HUANG Lan, JIANG Liang. Effect of hot extrusion and heat treatment on microstructure of nickel-base superalloy [J]. Transactions of Nonferrous Metals Society of China, 2014, 24(8): 2544–2553.
- [7] GAYDA J, GABB T P, KANTZOS P T. The effect of dual microstructure heat treatment on an advanced nickel-base disk alloy [C]//Superalloys. Pennsylvania: TMS, 2004: 323–329.
- [8] MAO J, CHANG K M, YANG W, RAY K, VAZE S P, FERRER D U. Cooling precipitation and strengthening study in powder metallurgy superalloy U720LI [J]. Metallurgical and Materials Transactions A, 2001, 32(10): 2441–2452.
- [9] JIA C L, GE C C, YAN Q Z. Microstructure evolution and mechanical properties of disk superalloy under multiplex heat treatment [J]. Materials Science and Engineering A, 2016, 659: 287–294.
- [10] PEI Zhong-ye, HAN Wei, ZHAO Gang, CHEN Xing-Fu, LI Jun-tao, TIAN Yan-wen. Effect of cooling rate on microstructure and mechanical properties of K465 superalloy [J]. Journal of Iron and Steel Research, International, 2009, 16(6): 70–74.
- [11] BEHROUZGHAEMI S, MITCHELL R J. Morphological changes of γ' precipitates in superalloy IN738LC at various cooling rates [J]. Materials Science and Engineering A, 2008, 498(12): 266–271.
- [12] MAO J, CHANG K M, YANG W, FERRER D U, RAY K, VAZE S P. Cooling precipitation and strengthening study in powder metallurgy superalloy Rene88DT [J]. Materials Science and Engineering A, 2002, 332(1): 318–329.
- [13] TIAN Gao-feng, JIA Cheng-chang, YIN Wen, LIU Guo-quan, HU Ben-hu. Cooling γ' precipitation behavior and strengthening in powder metallurgy superalloy FGH4096 [J]. Rare Matels, 2008, 27(4): 410–417.
- [14] TU Gan-yun, YANG Shi-zhong, WU Jian-tao. Effect of solution heat treatment on crack growth rate of P/M superalloy FGH 95 [J]. Transactions of Metal Heat Treatment, 1997, 18(3): 23–27.
- [15] ZHUANG X L, WU H Y, SI J Y, JIANG L. Influence of metallographic etchant on γ' precipitates characterization in a single crystal nickel-base superalloy [J]. Materials Science Forum, 2016, 849: 563–569.
- [16] FANG Jiao, LIU Chen-ze, LIU Jun, HUANG Lan, JIANG Liang. Analysis methods of phase transformation temperature on differential thermal analysis curves of powder metallurgy superalloy [J]. Transactions of Nonferrous Metals Society of China, 2015, 25(12): 3352–3360.
- [17] SINGH A R P, NAG S, CHATTOPADHYAY S, REN Y, TILEY J, VISWANATHAN G B, FRASER H L, BANERJEE R. Mechanisms related to different generations of γ' precipitation during continuous cooling of a nickel base superalloy [J]. Acta Materialia, 2013, 61(1): 280–293.
- [18] SINGH A R P, NAG S, HWANG J Y, VISWANATHAN G B, TILEY J, SRINIVASAN R, FRASER H L, BANERJEE R. Influence of cooling rate on the development of multiple generations of γ' precipitates in a commercial nickel base superalloy [J]. Materials Characterization, 2011, 62(9): 878–886.
- [19] MITCHELL R J, PREUSS M, TIN S, HARDY M C. The influence of cooling rate from temperatures above the γ' solvus on morphology, mismatch and hardness in advanced polycrystalline nickel-base superalloys [J]. Materials Science and Engineering A, 2008, 473(1–2): 158–165.
- [20] GABB T P, GAYDA J, KANTZOS P T, BILES T, KONKEL W. The tensile properties of advanced nickel-base disk superalloys during quenching heat treatments [C]//Fall Meeting. Indiana: TMS, 2001.
- [21] OJO A, CHATURVEDI M C. Liquefaction microfissuring in the weld heat-affected zone of an overaged precipitation-hardened nickel-base superalloy [J]. Metallurgical and Materials Transactions A, 2007, 38(2): 356–369.
- [22] LIU Xiao-tao, DING Han-hui, YANG Chuan, LIU Feng, HUANG Lan, JIANG Liang. Microstructure and mechanical properties of hot extruded FGH96 powder metallurgy superalloy [J]. Transactions of Nonferrous Metals Society of China, 2016, 26(2): 354–364.

冷速对一种镍基粉末高温合金的 显微组织和拉伸性能的影响

丁晗晖^{1,2}, 何国爱^{1,2}, 王薪^{1,2}, 刘锋^{1,2}, 黄岚^{1,2}, 江亮^{1,2}

1. 中南大学 粉末冶金国家重点实验室, 长沙 410083; 2. 中南大学 粉末冶金研究院, 长沙 410083

摘要: 研究不同淬火制度下晶粒尺寸及强化相 γ' 的尺寸分布、形貌和体积分数对镍基高温合金拉伸性能的影响。采用油淬和空冷两种淬火方式, 其对应的平均冷却速度分别为 183 °C/s 和 4~15 °C/s。实验结果表明, 油淬和空冷后的二次 γ' 相的平均尺寸分别为 24.5 nm 和 49.8 nm, 相应的体积分数分别为 29% 和 34%; 然而两种条件下的平均晶粒尺寸几乎相等。在室温下, 油冷态 γ' 相的拉伸强度高于空冷态的, 当温度升高到 650 °C 时, 二者强度逐渐接近。断口形貌分析表明, 在室温下, 断口由穿晶断裂主导; 随着温度升高, 直至 650 °C 以上, 断口由沿晶断裂主导。结果表明, 强化相 γ' 和晶界在镍基粉末高温合金中不同温度下发挥着不同的强化作用。

关键词: 镍基粉末高温合金; 冷却速度; 抗拉强度; γ' 沉淀相; 断裂机理

(Edited by Xiang-qun LI)